ARTICLES

The Allegro gravitational wave detector: Data acquisition and analysis

E. Mauceli, Z. K. Geng, W. O. Hamilton, W. W. Johnson, S. Merkowitz, A. Morse, B. Price, and N. Solomonson
Department of Physics and Astronomy, Louisiana State University, Baton Rouge, Louisiana 70803
(Received 8 December 1995)

We discuss the data acquisition and analysis procedures used on the Allegro gravity wave detector, including a full description of the filtering used for bursts of gravity waves. The uncertainties introduced into timing and signal strength estimates due to stationary noise are measured, giving the windows for both quantities in coincidence searches. [S0556-2821(96)01414-2]

PACS number(s): 04.80.Nn

I. INTRODUCTION

For the past ten years there has been little doubt that gravitational waves exist [1]. The extended series of measurements on the orbital decay of the binary pulsar have made it clear that angular momentum is radiating away from this system in agreement with the original predictions of Einstein. But the larger goal of direct detection of the waves and the development of such detection into gravitational wave astronomy still remains. Direct detection of gravitational radiation is a challenging experimental and technological problem. The current state of gravitational wave experimentation will allow detectors to record any predicted event that occurs within our galaxy and the technology is at hand to allow experimentalists to record events from remote galaxies. We report here on the data acquisition and analysis procedures used for the Allegro gravity wave detector, including the design of the optimal filter for burst signals and quantifying the uncertainties in estimating arrival times and signal strengths.

II. THE DETECTOR

Allegro is located in the Physics Building at Louisiana State University in Baton Rouge, Louisiana (30°25′N,91°10′W). It consists of a resonant bar equipped with a resonant inductive transducer and a dc superconducting quantum interference device (SQUID) amplifier all cooled to 4.2 K. It was operational from June 1991 until January of 1995 with a duty cycle approaching 95% and an average noise temperature (defined in Sec. IV) less than 6 mK. Figure 1 shows a schematic of the antenna.

A. The bar

The Allegro detector was designed to look for pulses of gravity waves such as those from the collapse of a massive star. Theoretical models (although varying widely in wave form and strength estimates) predict that stellar collapse to a neutron star or black hole would produce a burst of gravitational radiation with a duration on the order of milliseconds at frequencies near 1 kHz. For a resonant mass detector, a passing gravity wave deposits momentum into a massive elastic body, changing the amplitude and phase of the existing vibrational normal mode motion. The elastic body in the Allegro detector is a cylinder of aluminum alloy 5056, 60 cm in diameter and 300 cm in length. It has a physical mass of 2296 kg. Its first longitudinal normal mode is at 913 Hz. All cylinder detectors are most sensitive to signals propagating in a direction perpendicular to the bar axis. The bar is oriented perpendicular to the plane of the great circle on the earth that passes through Geneva, the location of the Rome Explorer antenna, and midway between Baton Rouge, LA and Stanford, CA. This orientation results in the axis of Allegro being directed along a line 40°24′ west of North. The Explorer detector of the University of Rome is perpendicular to the same great circle and as a result is parallel to Allegro. This means that a gravity wave should deposit the same amount of momentum into each of the detectors.

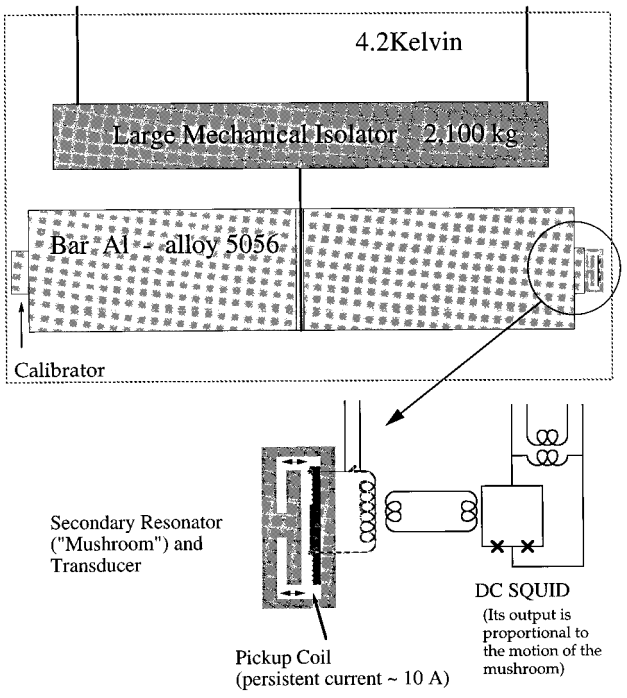

FIG. 1. The schematic of the Allegro antenna.

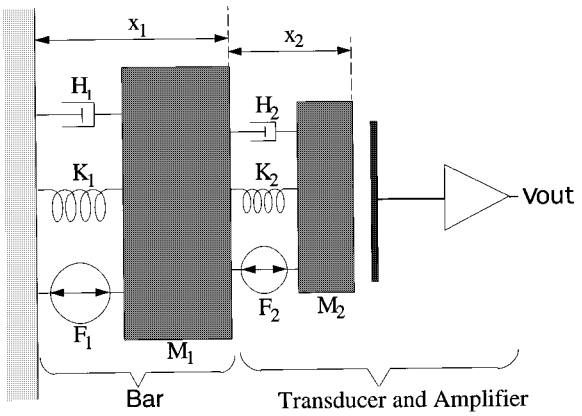

FIG. 2. A model of the Allegro antenna.

B. The transducer

Attached to one end of the bar is a smaller ''mushroom'' resonator resonant at the same frequency as the bar, thus making a two-mode system of coupled oscillators (referred to as the ''antenna'') [2,3]. The mass of the resonator is small enough so that the effects of a passing gravity wave on it are ignored. Facing the mushroom resonator but attached firmly to the bar is a superconducting pickup coil with a persistent supercurrent. The distance between the coil and the resonator is therefore proportional to the distance between the bar and resonator. Oscillations of the mushroom resonator change the inductance of the pickup coil, modulating the flux through it. A dc SQUID[1] converts the changing flux to a voltage.

C. The calibrator

An off-resonant capacitive transducer, the calibrator, is attached to the bar at the opposite end from the inductive transducer. Voltages applied to the capacitor applied forces to the antenna, which we used for a number of tasks. The calibrator was used to actively dampen the mode Q's to shorten the recovery time after large excitations and to cancel positive feedback on the antenna produced by the SQUID [3]. Under normal operating conditions the calibrator was used to excite the antenna at a frequency of 865.00 Hz, far removed from either of the modes. This ''continuous systems test'' provides a powerful tool for checking on the health of the detector. The calibrator was also used to provide burst signals to the antenna allowing the detector to be calibrated and allowing a study of the effects of noise on signal detection to be made.

D. The antenna model

The Allegro detector model is illustrated schematically in Fig. 2, where we include all of the relevant stationary noise sources. The equations of motion for this model are

$$M_1\ddot{x}_1(t)+H_1\dot{x}_1(t)+K_1x_1(t)-H_2\dot{x}_2(t)-K_2x_2(t)$$
$$=F_1(t)-F_2(t)+F_T(t)+\frac{1}{2}M_1L_1\ddot{h}_{xx}(t) \quad (1)$$

$$M_2[\ddot{x}_2(t)+\ddot{x}_1(t)]+H_2\dot{x}_2(t)+K_2x_2(t)=F_2(t)-F_T(t). \quad (2)$$

$M_{1,2}$ are the effective masses of the bar and mushroom resonator. L_1 is the effective length of the bar. $K_{1,2}$ represent the spring constants of the bar and mushroom resonator and $H_{1,2}$ their respective damping coefficients. $F_{1,2}$ are the Langevin force noise generators associated with the dissipation coefficients of each mass and F_T is the noise generated by a changing magnetic pressure from the superconducting pickup coil on the small mass resonator. x_1 is the amplitude of the first longitudinal normal mode of the bar, while x_2 is the relative displacement between the bar and the second resonator. The last term on the right hand side of Eq. (1) is the component of the gravitational wave tidal force along the bar axis.

The model shown does not explicitly include the superconducting circuitry or the SQUID. The voltage out of the SQUID is proportional to the relative displacement of the two masses:

$$V_{\text{out}}(t)=Gx_2(t)+\eta(t) \quad (3)$$

where G is a gain factor and $\eta(t)$ is white noise from the SQUID. The time response of the antenna to a large burst signal provided by the calibrator is shown in Fig. 3. The power spectrum of the stationary noise out of the SQUID is shown in Fig. 4(a). The two resonant modes, seen clearly in the figure, are at 896.8 Hz and 920.3 Hz. We refer to them as the minus and plus modes, respectively. Figure 4(b) shows the antenna response to a large burst signal and 4(c) shows the ratio of the noise to signal, which is the stationary noise treated as if it were due to a random flux of gravity waves exciting the bar.

III. DATA ACQUISITION

A. Signal demodulation

The voltage from the SQUID electronics is sent to a single lock-in detector which demodulates and low pass filters the signal. The reference frequency of the lock-in is set halfway between the normal mode frequencies of the antenna, thus shifting the frequency of the signal from the normal modes of the antenna to low frequency. Because the lock-in is set for a wide bandwidth, the frequency response of the detector over its entire bandwidth is monitored, enabling us to measure both the amplitude and phase of each of the resonant normal modes. It is due to the wide bandwidth that the continuous systems test can be applied to the antenna at a frequency far enough removed from the resonant modes as to not interfere with them. Other data collected to help monitor the detector include a direct low frequency signal from the SQUID, the status of the hardware and SQUID vetos, and signals from two seismometers, one of which is located on the floor next to the Dewar containing the antenna, the other on top of the vibration isolation table. A schematic of the data acquisition system in shown in Fig. 5.

[1]Biomagnetic Technologies, Inc., 4174 Sorrento Valley Blvd., San Diego, California 92121.

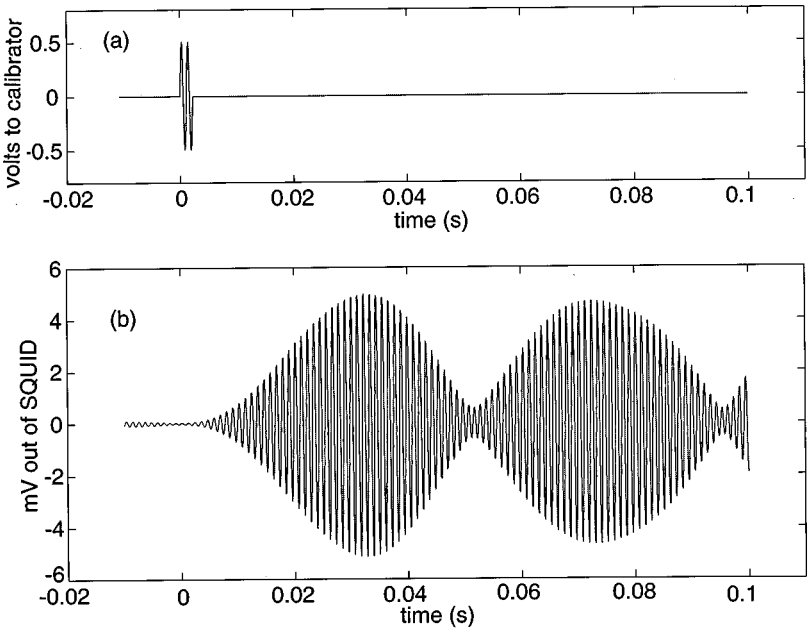

FIG. 3. Antenna response to a burst signal. (a) The voltage provided to the calibrator. (b) The voltage response out of the SQUID in the time domain.

The lock-in is an EG&G PAR 5210 two-phase lock-in amplifier with reference frequency set at 908.5220 Hz, although this changes if the mode frequencies shift by a couple of mHz. The reference signal is provided to the lock-in by a Hewlett Packard 3325A function generator equipped with a high stability oscillator. After the lock-in, the in-phase and quadrature output voltages are sent through an antialiasing filter (cutoff frequency 40 Hz) and then to the analog-to-digital interface box (A/D IB).

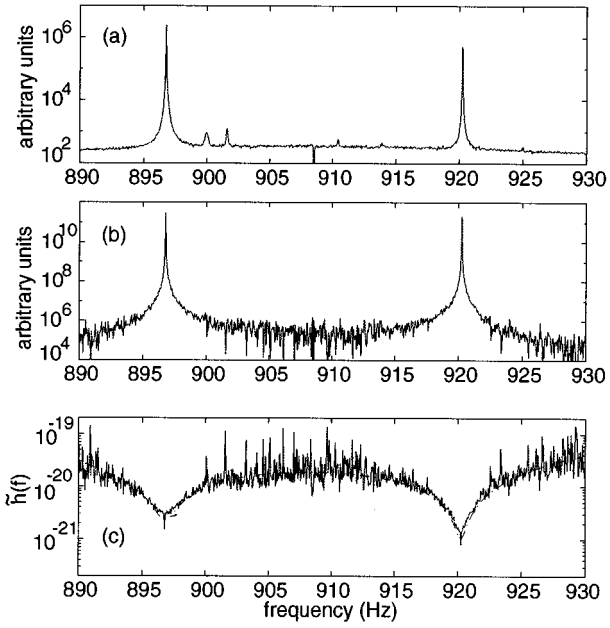

FIG. 4. (a) The power spectrum of the voltage out of the SQUID due to stationary noise sources acting on the antenna. (b) The power spectrum after the bar has been excited by a large burst signal. (c) The square root of the ratio of (a) and (b), showing the stationary noise as if it were all due to a random flux of gravity waves exciting the bar (strain noise). Also included in (c) is the strain noise predicted from the full Allegro model (dashed line).

B. Data collection

The A/D IB was constructed by the LSU Physics electronics shop and the Gravity Wave Group. It controls the sampling rate of the data, converts the analog signals to digital data streams, and sends the data to a VAXstation 3500. An important factor to note is that before any data were collected by the A/D IB rigorous testing was performed on it. A sine wave of amplitude large enough to span the entire range of the A/D converters was input to each A/D and the output inspected to verify (1) that the A/D converters responded properly, (2) that the time between samples remained constant and that no samples were missed, and (3) that the data written to disk were consistent with the input signal. It was not until the data acquisition system ran for about a week without any problems that it was considered stable enough to collect data.

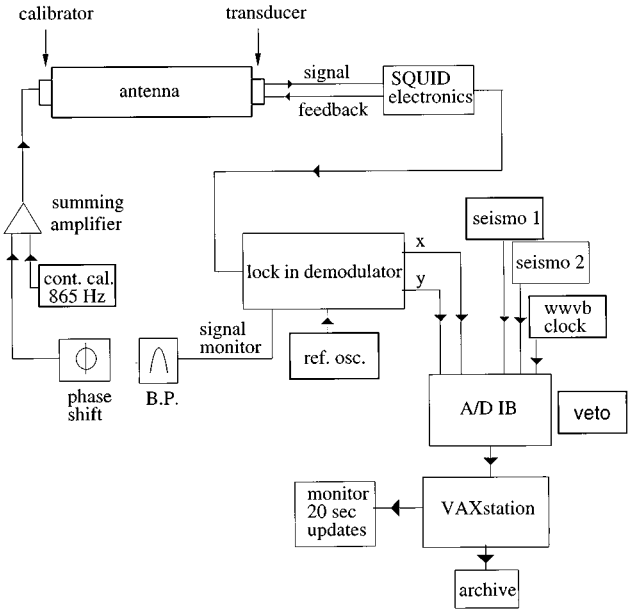

FIG. 5. Schematic of the Allegro data acquisition system.

TABLE I. Format of raw data record.

Once a record	
40 bytes	Header
2500 samples in a record of each of the following:	
2 bytes	lock-in output x
2 bytes	lock-in output y
2 bytes	2 seismometer outputs (12-bit resolution each)
2 bytes	4 veto bits and 12 bits low frequency SQUID output
2 bytes	universal time (unit seconds + milliseconds) (BCD encoded)
In the header	
2 bytes	UT day number
1 byte	File identifier (A, . . . ,Z)
1 byte	block type
2 bytes	record number in file (1, . . . ,4320)
2 bytes	run number
8 bytes	VMS time of the first sample in the block
6 bytes	spare
4 bytes	university identification
2 bytes	universal time of the first sample in the block
2 bytes	UT word 1
2 bytes	UT word 0
2 bytes	gain code
2 bytes	sampling time
2 bytes	number of samples in a block
2 bytes	number of lock-ins

A Kinemetrics model 60-DC clock provides a 1 kHz square wave phase locked to coordinated universal time (UTC) which the A/D IB uses as a counter. When the counter reaches 8 ms the data are sampled and sent to disk, resulting in a sampling time of 8 ms. Data sampled include (1) the in-phase and quadrature output channels of the lock-in (referred to as x and y, respectively), (2) a direct low frequency signal from the SQUID, (3) the signal from the two seismometers, (4) the status of the hardware and SQUID vetos, and (5) the sample time in UTC. The voltages out of the lock-in are sampled with 16-bit accuracy, the others with 12-bit accuracy. These data are referred to as the raw data to denote that they have not been subject to any software fiddling. Table I shows the format of the raw data in a record. Twenty seconds worth of data (2500 samples) is assembled by software into a data block and written to disk. There are 4320 blocks in a full day's worth of data. A DEC 3000 AXP, clustered to the VAXstation 3500, is used for on-line monitoring of the detector and analysis of the data. A week's worth of data (about 875 Mbytes) are allowed to accumulate on disk and are then archived to 4 mm DAT tape. Two tapes are made using VMS BACKUP to ensure the data are transferred accurately and one tape is made using VMS COPY which allows easy access to the data. One BACKUP tape and the COPY tape are stored in the lab, while the other BACKUP tape is stored off campus.

IV. DATA ANALYSIS

The data analysis programs read a block of data directly off the disk. Since the data are written to disk every 20 s, they are available 20 s or less after being collected. In this way problems with the detector or with the electronics can be identified and corrected quickly. This ''on-line'' monitoring capability does not affect the taking of data since it is a separate program running at a much lower priority than the collection routine.

A single program, written in the language MATLAB,[2] does the majority of the data analysis. The analysis begins by reading in a block of data, removing dc offsets from the in-phase and quadrature signal components, and correcting for lock-in gain. The program implements two digital lock-ins which mix x and y with reference frequencies set at the plus and minus resonant frequencies. The outputs of these digital lock-ins are the in-phase and quadrature components of the amplitude of each mode, written as x_+, x_-, y_+, and y_- where $+$ refers to the plus mode and $-$ the minus. The in-phase and quadrature components of each mode are then separately filtered with an eighth order digital Bessel anti-aliasing filter having a corner frequency of 2.35 Hz. The filtered data are then decimated to reduce the amount of data handling. We keep only every tenth sample, truncating the data to an effective sampling time of 80 ms.

The in-phase and quadrature components of each mode are optimally filtered for a burst signal (see Sec. V) and the output squared and added to form the mode burst energies at each sample. Representing the output of the optimal filter by

[2]The MathWorks, Inc. 24 Prime Park Way, Natick, Massachusetts 01760.

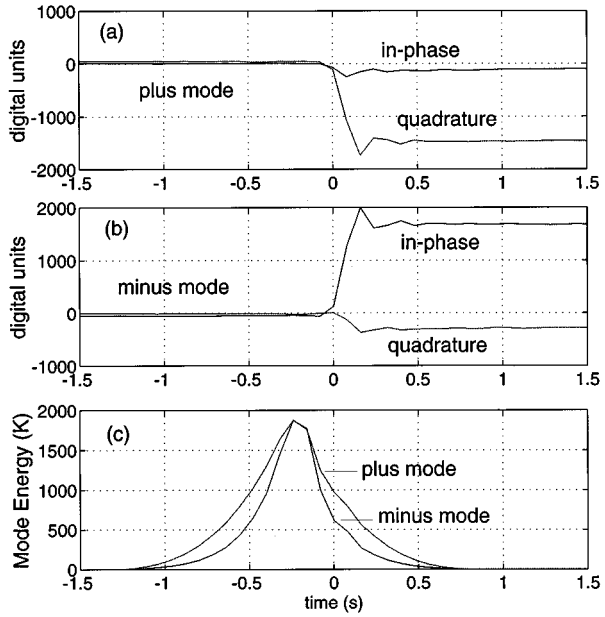

FIG. 6. (a) The plus and (b) the minus mode amplitudes in response to the signal of Fig. 3. (c) The optimally filtered response to the same signal.

f_{x+}, f_{y+}, f_{x-}, and f_{y-}, the estimate of the burst energy at each sample is

$$E_{\pm}=f_{x\pm}^2+f_{y\pm}^2. \tag{4}$$

The mode response to a large burst both before and after optimal filtering is shown in Fig. 6.

It has become conventional in this field to express energy in kelvin. Therefore, a ''mode noise temperature'' is defined as the mean value of the mode burst energy $T_{\pm}=\langle E_{\pm}\rangle/k_B$. Burst energy is not to be confused with the energy in a mode as given by the equipartition theory. Instead, it is a measure of the change in energy of the modes between samples. Since the sampling time is much less than the ''random walk'' time of the antenna (8 ms compared to 40 min) the noise temperature is much less than the physical temperature of 4.2 K.

To reduce the amount of data handled, a threshold is applied so that only those samples with energy ten times the noise temperature or greater in both modes are recorded each day by the analysis programs. Each sample is tagged with the time in seconds from the start of the day. Above this threshold there are roughly 400–600 Allegro samples per day (Fig. 7). Also, as part of the analysis the average over each record of x_+, x_-, y_+, y_-, E_+, and E_- is recorded along with the UTC time of the start of each record and the raw low frequency and seismometer data. This information is used primarily for diagnostic checks on the detector.

This is the end of the analysis unless there is to be a coincidence search with other gravity wave detectors, such as the Explorer detector of the University of Rome, or Gamma Ray Observatory (GRO) γ-ray data. Before exchanging data, we first edit those excitations of the antenna that can be positively identified as something other than a gravity wave (such as an earthquake or an electronic hiccup). Next, the mode noise temperatures (Fig. 8) are calculated in six minute averages for the entire span of the coincidence search. The statistically correct way to combine the energy information from both modes is by forming a weighted burst energy:

$$E_w=T_w(E_+/T_++E_-/T_-) \tag{5}$$

where

$$T_w^{-1}=T_+^{-1}+T_-^{-1} \tag{6}$$

is the weighted noise temperature (this is the overall noise temperature of the detector) and T_+ and T_- are the previously mentioned averages.

A threshold is applied to E_w so that only samples with $E_w>11.5T_w$ are kept. The factor of 11.5 was chosen so that the Allegro event rate for the 1991 coincidence search with

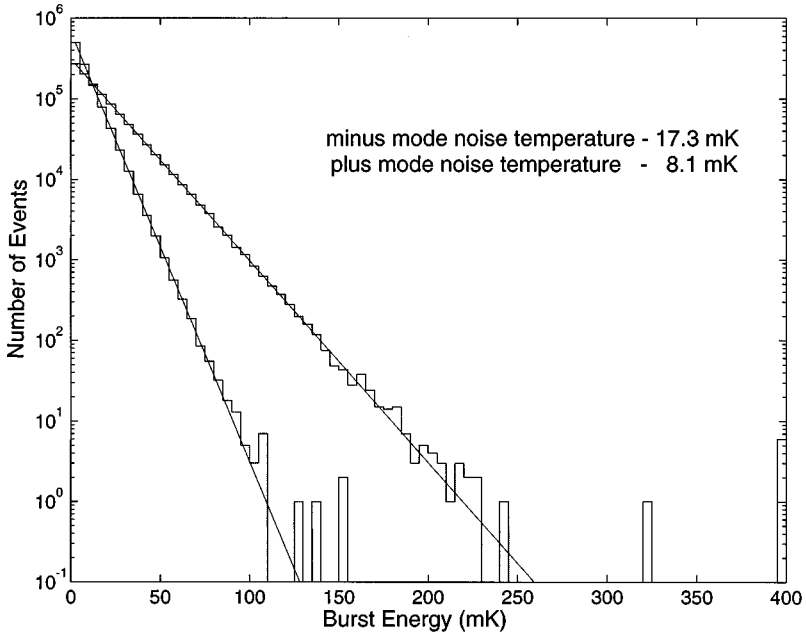

FIG. 7. A histogram of the energy in each mode for day 200 of 1994. The slope of the histogram gives the noise temperature for each mode.

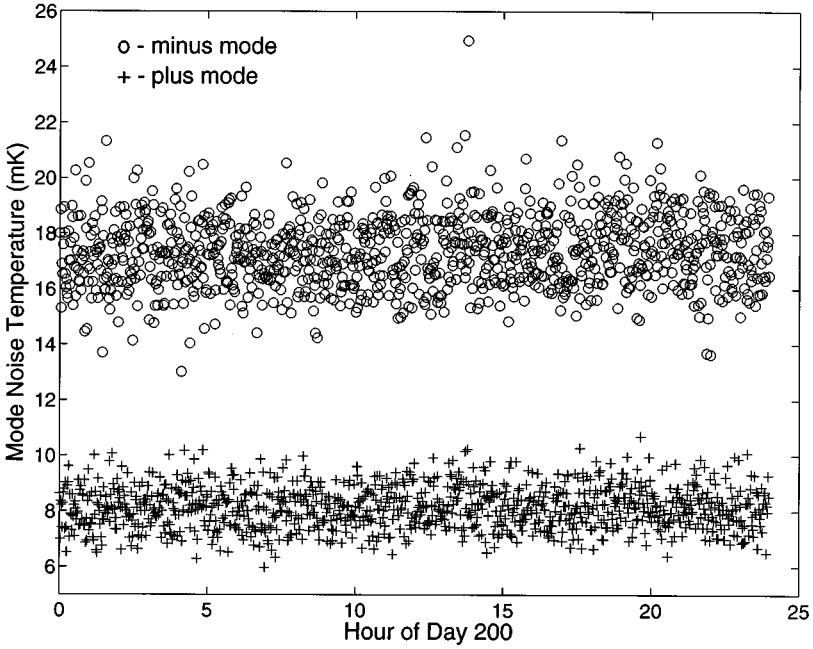

FIG. 8. The average noise temperature in each mode during day 200 of 1994. Each data point represents a six minute average of the mode burst energies.

the Explorer detector would be about 100 events/day. The consistency of the Allegro detector is demonstrated by the fact that the same threshold produced about 100 events/day for the entire 3 1/2 years of continuous operation. Consecutive samples above threshold are then collapsed into a single time and energy, creating an event. The energy assigned to the event is the energy of the sample in the series of consecutive samples above threshold with the maximum energy value. The time of the event is given by the time of the first sample in the series plus half the duration of the series, where the duration is defined to be the time of the last sample minus the time of the first sample. The sample time is determined by reading the UTC time at the beginning of the record containing the event and then counting the number of samples (at 80 ms between samples) into the record to that event. Then an offset is subtracted from the resulting time to account for filtering delays. Figure 9 shows the final event list for a small section of data.

V. THE FILTERING ALGORITHM

The optimal filtering on Allegro is done in the time domain so that it can be applied directly to the incoming data. We use the MATLAB filter routine which applies the optimal filter to the data using the transposed direct form II structure [4, p. 155]. The filter coefficients which will maximize the signal to noise ratio for a sequence of data involving stationary noise are given by [[5], pp. 183–184, [6], pp. 126–135]

$$\underline{a} = \underline{\underline{R}}^{-1}\underline{s} \tag{7}$$

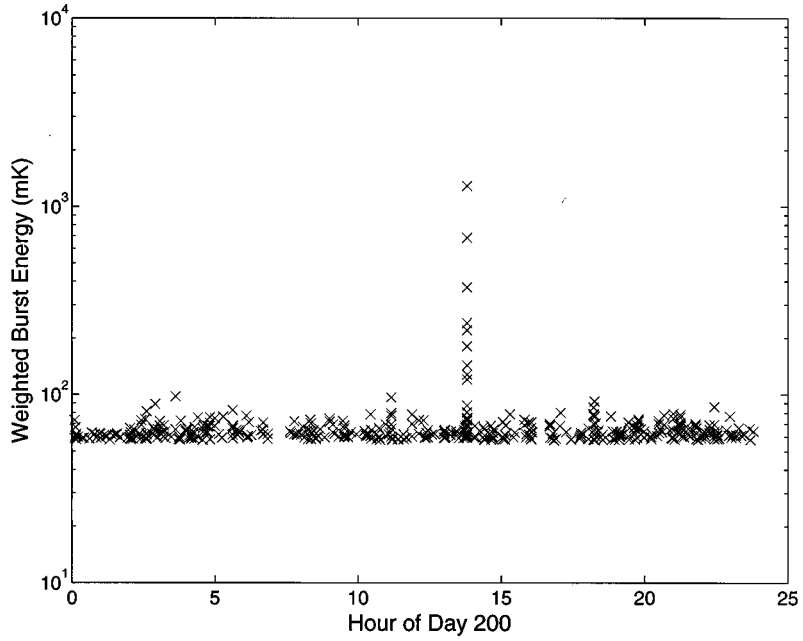

FIG. 9. The final event list for day 200 of 1994.

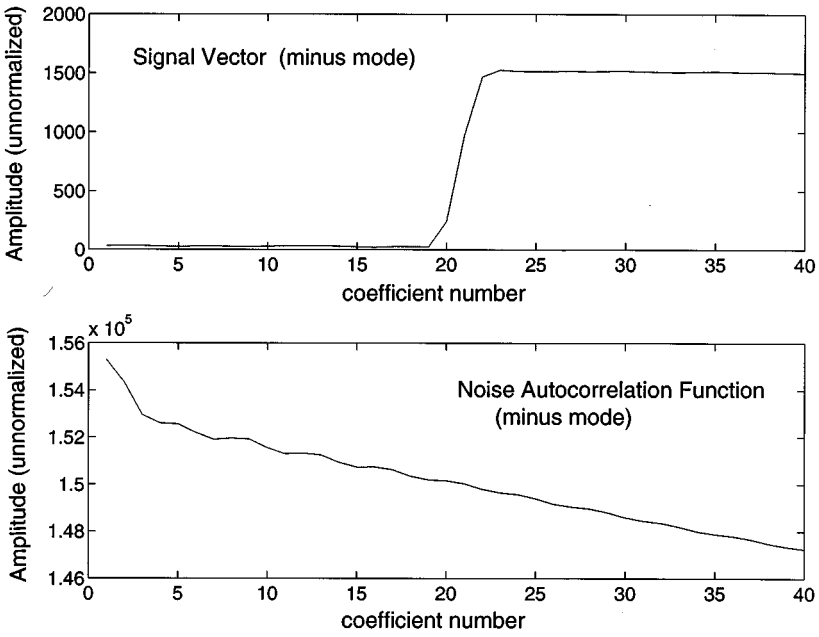

FIG. 10. The signal vector and noise autocorrelation function used in creating the optimal filter for the minus mode.

where $\underline{q}$ is the vector containing the filter weights, $\underline{\underline{R}}^{-1}$ is the inverse of the autocorrelation matrix of the noise, and $\underline{s}$ is the detector's response to the signal being looked for. In the following analysis of the optimal filter we will use a single underline to denote a vector and two underlines for a matrix. Because the in-phase and quadrature components for each mode are statistically similar, they can be averaged to make a single correlation function for the noise in each mode. Also, the in-phase and quadrature components of the signal vector are combined (described later) to form the mode response to a burst. The correlation functions of the two modes are not similar and therefore a pair of filter weights is created, one to filter the plus mode and the other to filter the minus mode. The details of creating the autocorrelation matrix and the response vector (signal) are described next.

A. The signal

The signal vector $\underline{s}$ is obtained by applying a very large calibration pulse to the antenna so that the low pass filtered and decimated output is essentially unaffected by the stationary noise. Next, the mean value of the first few samples is subtracted from each sample in the signal array so that the amplitude just before the pulse hits the antenna is near zero. Then, the squares of the in-phase and quadrature signal components in each mode are added and the square root taken to create the final form of the signal vector (Fig. 10):

$$\underline{s_{\pm}} = \sqrt{(\underline{s_{\pm}^{x}})^2 + (\underline{s_{\pm}^{y}})^2}. \tag{8}$$

B. The noise

The first step in forming the autocorrelation matrix for the noise is to form the autocorrelation function for one record's worth of low pass filtered and decimated data,

$$\underline{R} = \frac{1}{N}\sum_{i=0}^{N-1} n_i n_{i+j}, \tag{9}$$

with N the number of coefficients in the filter, i the sample index, and j the time offset index. This is done every 20th record for an entire day's worth of data. It is necessary to use such a long time span of data because of the long relaxation times of the normal modes. All events outside the thermal distribution are removed from the data before forming the correlation function as the presence of nonstationary noise will degrade the filter's performance. The length of the filter, N, was determined experimentally. Filter lengths of 20 to 50 decimated samples were tried and it was found that the noise temperature of the modes decreased up to 40 coefficients (amounting to 3.2 s of data). After that, the noise temperature no longer decreased with increasing coefficient number so 40 decimated samples was chosen as the length for the filter.

Next, the values of $\underline{R}$ at each j from each record analyzed are summed and the in-phase and quadrature components added to form the autocorrelation function for a mode. The autocorrelation matrix is formed using the Matlab routine toeplitz such that the zero delay components R_{00} lie along the diagonal:

$$\underline{\underline{R_{\pm}}} = \text{toeplitz}[\tfrac{1}{2}(\underline{R_{\pm}^{x}} + \underline{R_{\pm}^{y}})]. \tag{10}$$

Here the in-phase and quadrature components are denoted with an x and y, respectively. The inverse of the matrix is formed using the MATLAB inv routine:

$$\underline{\underline{R_{\pm}}}^{-1} = \text{inv}(\underline{\underline{R_{\pm}}}). \tag{11}$$

Having obtained the inverse of the autocorrelation function for the noise and the signal vector, the filter weights for both the plus and minus modes are formed by Eq. (7). The final form of the weights is shown in Fig. 11.

C. Normalization

Once the optimal filter is constructed the weights are normalized by putting a pulse of known energy into the antenna using the calibrator. An SRS Model DS345 function generator was used to provide 2 cycles of a 908 Hz sine wave of

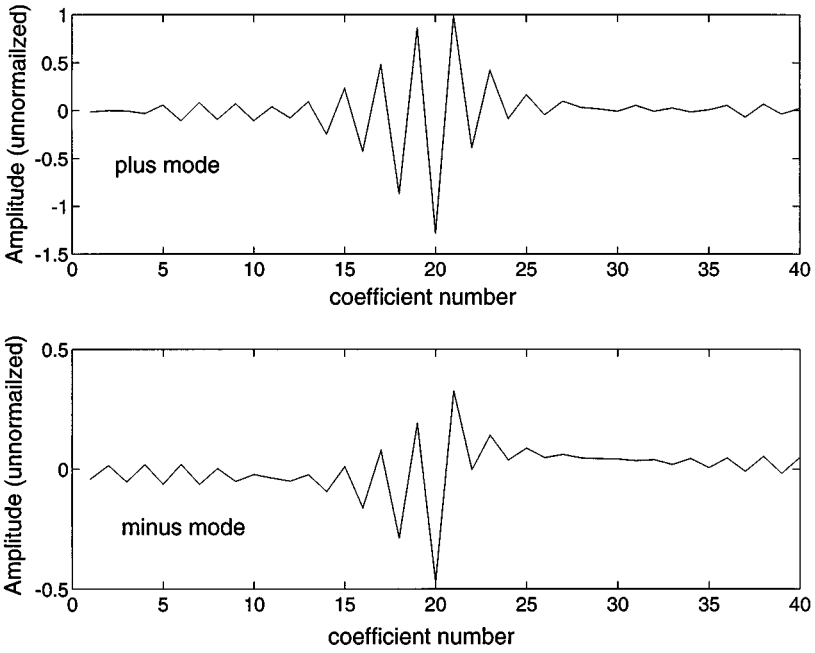

FIG. 11. The optimal filter weights for the minus and plus modes.

constant amplitude to the calibrator at 20 s intervals. The energy deposited in each mode of the antenna by a single pulse is [7]

$$E_{\mathrm{cal}\pm}=\frac{\pi}{2}\frac{\gamma_{\pm}}{\omega_{\pm}}(NV)^2 \tag{12}$$

where $\gamma_{\pm}$ is the calibrator coupling coefficient for each mode, defined as the ratio of the current output from the calibrator to the input driving voltage and were measured in a separate experiment. $\omega_{\pm}$ are the mode frequencies, N is the number of cycles, and V is the voltage zero to peak provided to the calibrator. A weighted burst energy is formed with Eq. (5).

Approximately 60 pulses were applied having an amplitude large enough so that the effects of stationary noise on the estimate of the resulting burst energies was small. After applying the pulses the data was analyzed as described in Sec. IV to produce a list of corresponding events. The mean of the mode burst energies of the pulses was compared to the expected energy deposited in the antenna as given by Eq. (12) and the filter weights scaled so that the two matched.

The filtering scheme causes a delay between the actual arrival time of a pulse and the recorded arrival time. This delay needs to be measured and removed from the estimate of the timing of events. A very large calibration pulse was applied to the antenna and analyzed to produce a filtered event. This event consisted of approximately 40 decimated samples similar to Fig. 6. The time ascribed to this event by the procedure described previously was 14 581.672 s. Examining the raw data (after lock-in and low pass filtering but before any processing by the analysis programs or decimation) it was determined that the first signs of the calibration pulse affecting the antenna appeared at 14 579.936 s. Subtracting the two gives a delay of 1.74 s, which is then removed when the event times are recorded.

VI. EVENT UNCERTAINTIES

It is impossible for a single detector to differentiate between a gravity wave passing through the antenna and excitations due to noise. At low energies the thermal spectrum (stationary noise) masks any signal, while above that a signal is indistinguishable from a burst of nonstationary noise. Two or more (the more the better) detectors operating in coincidence, however, can greatly reduce the noise level by demanding that (1) a gravity wave excite each antenna simultaneously within a few milliseconds, depending on the distance between them and (2) for similar detectors aligned with respect to astrophysical sources, such as Allegro and Explorer, the energy deposited in each be equal. Unfortunately, noise sources add a degree of uncertainty to any measurements of event arrival time and energy with the result that one looks instead for a coincidence (1) in a window of time which is much greater than the light travel time between detectors and (2) where the energy of a signal is no longer equal in each detector, but lies in some range which we shall show depends on both the noise temperature of the detectors and the strength of the signal. In this section we quantify the

TABLE II. The anticipated energy of each calibration pulse and the number of pulses applied at that energy for a given series.

Calibration series	Pulse energy (mK)	Number of pulses
cal2_312	64	100
cal3_312	76	100
cal4_312	110	100
cal1_317	220	100
cal2_317	420	100
cal3_317	1000	100
cal1_327	110	60
cal2_327	150	60
cal3_327	220	60

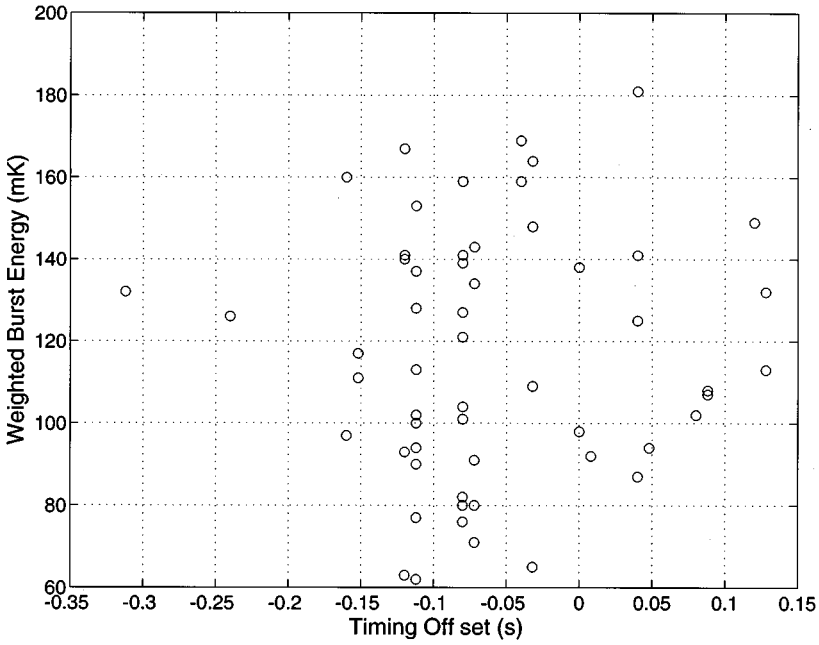

FIG. 12. The burst energy associated with each calibration pulse in series cal1_327 and the corresponding timing offset. The shift away from zero delay is common to all calibration series having a mean value of $\leqslant 0.06$ s.

uncertainties introduced into these measurements by the stationary noise.

Using the same parameters as described in Sec. V a series of calibration pulses was applied to the bar. A signal from the function generator was connected to one channel of the hardware veto so that at the same time a voltage pulse was applied to the calibrator a veto was recorded. This allowed the sample immediately following excitation of the antenna to be identified. The largest error this procedure can produce in the timing of the pulse is 8 ms, which, as we shall see, is much smaller than the final uncertainties in the timing. The anticipated energy deposited by each pulse given by Eq. (12) and their number for each calibration series are shown in Table II.

A. Uncertainties in timing

The calibration pulses were analyzed with the procedures described in Sec. IV to produce lists of event times and energies. Call the event time assigned to each calibration pulse the ''arrival time'' and identify a ''pulse application time'' with the tripping of the veto. Subtracting the arrival time from the application time produces a timing offset for each calibration pulse. Figure 12 shows the offset for each pulse in the calibration series cal1_327. The standard deviation of the offsets is a measure of the uncertainties in our timing procedures. Figure 13 shows the standard deviation of the offsets from each series of pulses, in effect plotting the timing uncertainty as a function of signal strength. Of the nine data points shown, seven are within one standard deviation of the mean uncertainty, and only the smallest signal (still

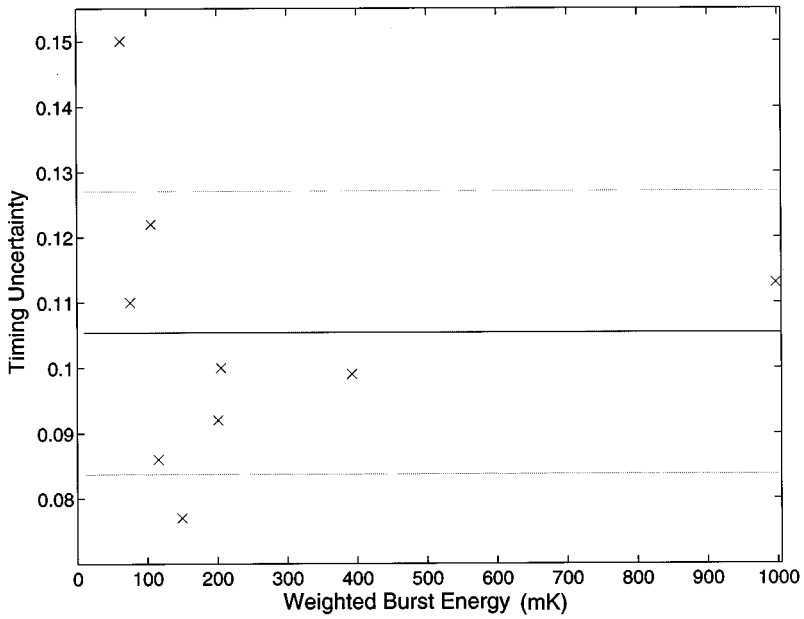

FIG. 13. The uncertainty in the timing for each calibration series (defined as the standard deviation of the offsets) is represented by the crosses. The solid line in the mean value of the timing uncertainties. The dotted lines are one standard deviation away from the mean value of the nine data points plotted.

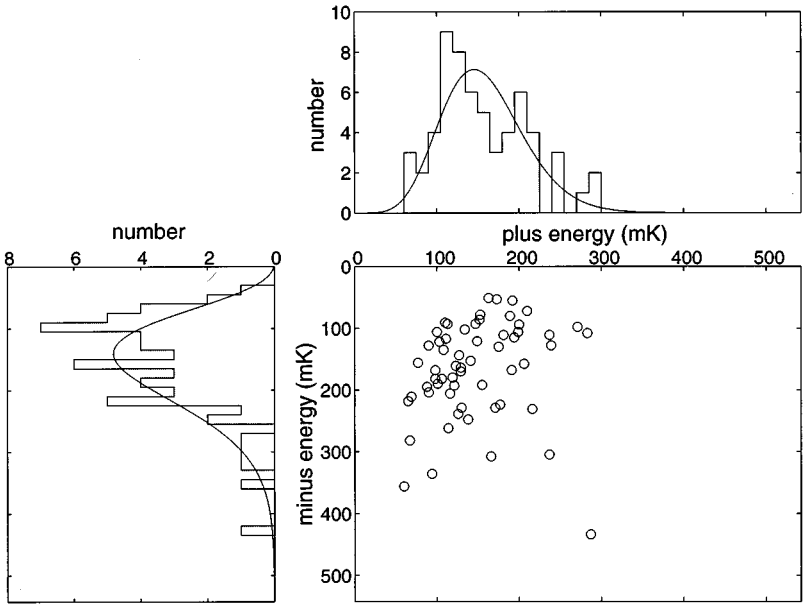

FIG. 14. The estimate of the energy deposited in the plus mode plotted against that in the minus mode for each pulse in the calibration series cal2_327 . Sharing the same axis are histograms of the mode burst energies and the distribution function of Eq. (15).

about $11.5T_w$) is significantly different. What is surprising is that at the highest signal strength, about $180T_w$, the timing is no more accurate than at lower energies. The end result is that for signals above $11.5T_w$ Allegro's timing is accurate to ± 0.1 s.

B. Uncertainties in energy

Noise sources acting on the antenna, both thermal and electronic, are stationary distributed with zero mean. This property is not changed by either the lockin or the optimal filtering. In the absence of a signal or nonstationary noise the outputs from the optimal filter are statistically independent zero mean stationary variables with variance $\sigma_{\pm}^2$. Forming the mode energies by Eq. (4) results in an exponential distribution

$$p(E_{\pm}) = \frac{1}{T_{\pm}} \exp\left(\frac{E_{\pm}}{-T_{\pm}}\right) \tag{13}$$

with $E_{\pm}$ the detector response to stationary noise and $T_{\pm} \equiv 2\sigma_{\pm}^2$. This distribution has a nonzero mean given by

$$\langle p(E_{\pm}) \rangle = T_{\pm} . \tag{14}$$

If a signal of burst energy $E_{\mathrm{cal}\pm}$ is present, it can be shown that the mode burst energy of the signal combined with the stationary noise is noncentral χ^2 distributed with two degrees of freedom [6];

$$p(E_{\pm}) = \frac{1}{T_{\pm}} \exp\left(\frac{(E_{\pm} + E_{\mathrm{cal}\pm})}{-T_{\pm}}\right) I_0\left(\frac{2\sqrt{E_{\pm} E_{\mathrm{cal}\pm}}}{T_{\pm}}\right) \tag{15}$$

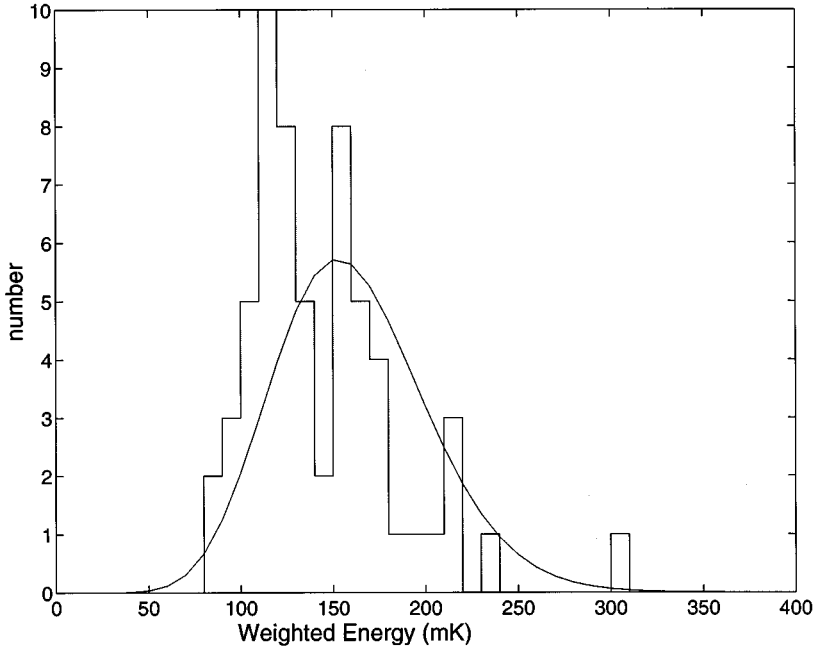

FIG. 15. The histogram of the weighted burst energies for the calibration series cal2_327 and the distribution function of Eq. (18).

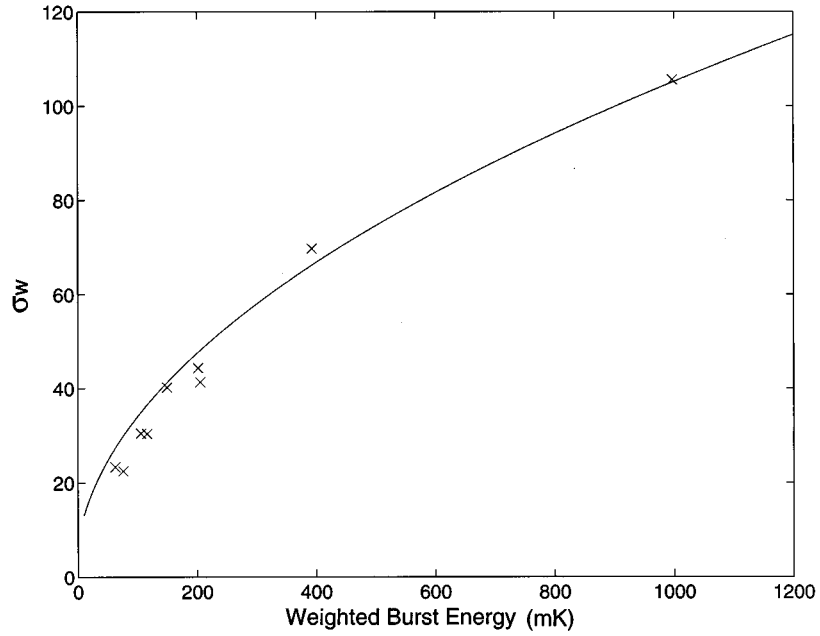

FIG. 16. The spread in the burst energy of a signal due to stationary noise. Each data point is the standard deviation of the energy estimates for a calibration series. The solid line is a theoretical curve generated from the square root of Eq. (20) with a noise temperature of 5.5 mK.

where I_0 is the modified Bessel function of zeroth order. The mean and variance of this distribution are given by

$$\langle p(E_{\pm})\rangle = E_{\mathrm{cal}\pm} + T_{\pm}\,, \tag{16}$$

$$\mathrm{var}(p_{\pm}) = 2E_{\mathrm{cal}\pm}T_{\pm} + T_{\pm}^2\,. \tag{17}$$

The weighted energy as defined in Eq. (5) is fourth order noncentral χ^2 distributed [6] with noncentral parameter equal to the weighted burst energy E_{cal}:

$$p(E_w) = \frac{1}{T_w}\exp\left(\frac{(E_{\mathrm{cal}}+E_w)}{-T_w}\right) I_1\left(\frac{2\sqrt{E_w E_{\mathrm{cal}}}}{T_w}\right)\sqrt{\frac{E_w}{E_{\mathrm{cal}}}} \tag{18}$$

where E_w is the weighted burst energy due to the stationary noise. The mean and variance are given by

$$\langle p(E_w)\rangle = E_{\mathrm{cal}} + 2T_w\,, \tag{19}$$

$$\mathrm{var}(p_w) = 2E_{\mathrm{cal}}T_w + 2T_w^2\,. \tag{20}$$

Both the distribution for the mode burst energy and the weighted burst energy are described by only two parameters, the size of the signal and the noise temperature of the detector. That the actual data from the detector follow these distributions is shown in Fig. 14 and Fig. 15.

Equation (20) is the important result with regards to a coincidence search. If we identify the spread in energy due to the interaction with the noise as the square root of Eq. (20), call it σ_w, then for a given noise temperature the spread increases as the square root of the signal strength. Figure 16 demonstrates that the data from Allegro match the theory well. This curve is used to define the window of a coinci-

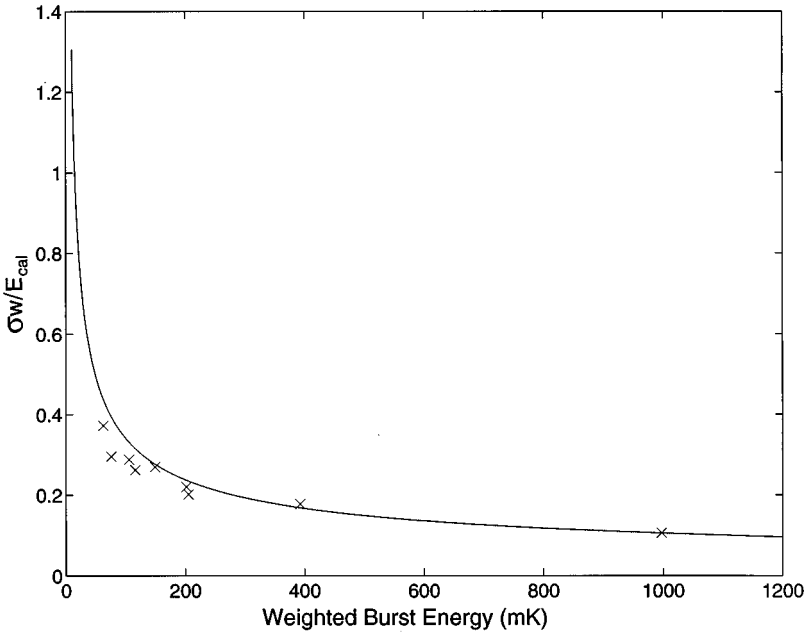

FIG. 17. The fractional spread in burst energy of a signal mixed with stationary noise. This is simply the results of Fig. 16 divided by the mean value of the burst energy.

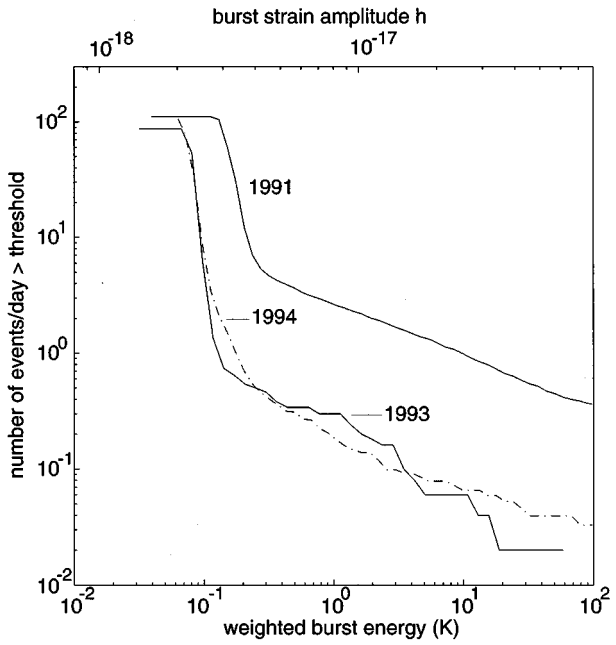

FIG. 18. Allegro energy spectrum for 1991, 1993, and 1994. The bottom scale gives the signal threshold in kelvin, the top scale gives the signal threshold in terms of the burst strain amplitude of a gravity wave incident with optimum polarization and direction.

dence in energy. Although the spread increases with increasing signal strength, the fractional change in energy, defined as $\sigma_w/E_{\rm cal}$, decreases as $1/\sqrt{E_{\rm cal}}$ as is shown in Fig. 17.

VII. NONSTATIONARY NOISE

The previous section dealt with the effects of stationary noise on the accuracy of the event parameters time and energy. There is another class of noise, nonstationary noise, which affects the running of the detector as an observatory. Figure 18 shows the Allegro energy spectra from 1991, 1993, and 1994. Each spectrum is divisible into two parts, the low energy stationary noise and the background events which could be from any number of mechanisms related to the detector or surroundings, or could be from gravity waves. The lowering of the background from 1991 to 1993 is attributed to two causes. First, the antenna was warmed to 15 K at the beginning of 1993, which may have reduced trapped flux in the superconductors or released some built up mechanical stress. Second, there were a number of background sources identified after 1991: millisecond electrical transients, earthquakes from around the globe, and buses hitting a pothole outside the physics building. Examining the raw data associated with each event outside of the thermal distribution allowed events produced by these sources to be easily recognized and vetoed with only a slight increase in the detector dead time.

VIII. CONCLUSION

We have described the data acquisition and analysis procedures of the Allegro gravity wave detector. The creation of an optimal filter to look for burst signals was discussed in detail, and the uncertainties in assigning a time and energy to an event due to stationary noise were calculated and shown to match the data, setting the windows for both quantities in coincidence searches.

ACKNOWLEDGMENTS

This research was supported by the National Science Foundation under Grant No. PHY-9311731.

[1] J. H. Taylor and J. M. Weisberg, Astrophys. J. **345**, 434 (1989).
[2] H. J. Paik, Ph.D. dissertation, Stanford University, 1974.
[3] N. Solomonson, W. O. Hamilton, and W. Johnson, Rev. Sci. Instrum. **65**, 174 (1994).
[4] A. V. Oppenheim and R. W. Schafer, *Digital Signal Processing* (Prentice-Hall, Englewood Cliffs, NJ, 1975).
[5] L. A. Wainstein and V. D. Zubakov, *Extraction of Signals from Noise* (Dover, New York, 1962).
[6] A. D. Whalen, *Detection of Signals in Noise* (Academic, New York, 1971).
[7] S. Boughn *et al.*, Rev. Sci. Instrum. **61**, 1 (1990).